Sea level rise and tidal power plants in the Gulf of Maine

Pelling, H.E.; Green, J.A.

Journal of Geophysical Research

[Cyswllt i'r cyhoeddiad / Link to publication](#)

09. Oct. 2020

Sea level rise and tidal power plants in the Gulf of Maine

Holly E. Pelling[1] and J. A. Mattias Green[1]

[1] The response of the Bay of Fundy and Gulf of Maine to large-scale tidal power plants and future sea-level rise is investigated using an established numerical tidal model. Free stream tidal turbines were simulated within the Bay of Fundy by implementing an additional bed friction term, K_t. The present-day maximum tidal power output was determined to be 7.1 GW, and required $K_t = 0.03$. Extraction at this level would lead to large changes in the tidal amplitudes across the Gulf of Maine. With future SLR implemented, the energy available for extraction increases with 0.5–1 GW per m SLR. SLR simulations without tidal power extraction revealed that the response of the semidiurnal tides to SLR is highly dependent on how changes in sea level are implemented in the model. When extensive flood defenses are assumed at the present-day coast line, the response to SLR is far larger than when land is allowed to (permanently) flood. For example, within the Bay of Fundy itself, the M_2 amplitude increases with nearly 0.12 m per m SLR without flooding, but it changes with only 0.03 m per m SLR with flooding. We suggest that this is due to the flooding of land cells changing the resonant properties of the basin.

1. Introduction

[2] The tides of the Gulf of Maine (Figure 1) are some of the largest in the world with an observed tidal range of some 16 m in the Bay of Fundy due to resonance of the semidiurnal tides [e.g., *Garrett*, 1972]. This very large tidal range makes the Bay of Fundy a desirable location for large-scale tidal power plants (henceforth "TPP"; see e.g., *Garrett* [1972] and *Greenberg* [1979] for details about the bay], but at the same time the near resonant state of the bay makes the system sensitive to perturbations of the basin [*Ray*, 2006; *Karsten et al.*, 2008]. Furthermore, the near-resonant properties of the Bay of Fundy in combination with its location—close to where the tidal wave enters the Gulf of Maine from the North Atlantic—ensures that any changes to the tides within the bay will have back effects far into the Gulf of Maine [*Müller*, 2011]. The sensitivity of the tidal system in the Gulf of Maine therefore opens for a fundamental question: how will the tide change in the Gulf of Maine if tidal power is extracted within the Bay of Fundy in combination with large levels of future sea-level rise (SLR)?

[3] The large tidal range of the Gulf of Maine has attracted the attention of renewable energy industries, keen on exploiting this natural resource. However, the tides in the Gulf are extremely sensitive to the implementation of TPP due to feedbacks induced by the increased dissipation of tidal energy [*Garrett and Cummins*, 2005; *Sutherland et al.*, 2007]. For example, *Karsten et al.* [2008] showed that the placement of a free stream TPP in Minas Passage could affect the tides as far away as the Bay of Boston (Figure 1). Also, because TPP are designed to have a working lifespan of some 120 years [*Woollcombe-Adams et al.*, 2009], they will operate in an environment which may experience SLR, and the combined response of the tides to SLR and TPP is unknown. Here, we therefore ask how will TPP and SLR change the tides in the Gulf of Maine if they are implemented individually and in combination?

[4] The current estimate of present global SLR is approximately 1.9mm yr^{-1} and this is expected to accelerate over the present century [*Church and White*, 2006, 2011; *Woodworth et al.*, 2011]. Surprisingly, even the moderate SLR (a fraction of a meter) the ocean has experienced over the last few decades has already had an impact on regional tidal systems [e.g., *Woodworth et al.*, 2009; *Müller et al.*, 2011]. The SLR of 0.2–2 m estimated for the year 2100 [*Denman et al.*, 2007; *Rahmstorf*, 2007] may therefore have a large impact on regional tides [e.g., *Müller et al.*, 2011; *Pickering et al.*, 2012; *Ward et al.*, 2012]. Tide gauge data show that sea level in the Gulf of Maine has already risen some 30 cm between 1880 and 1980, but that the rate had dropped to 20 cm per century over the past 30 years [*Greenberg et al.*, 2012]. We may thus expect a significant change in sea level within the area over the life span of a potential TPP in the Bay of Fundy. *Greenberg et al.* [2012] also show that tidal high water is likely to

---

[1]School of Ocean Science, College of Natural Science, Bangor University, Menai Bridge, LL59 5AB, UK.

Corresponding author: H. E. Pelling, School of Ocean Science, College of Natural Science, Bangor University, Menai Bridge LL59 5AB, UK (osp807@bangor.ac.uk)

significantly increase over the next century, due to a combination of ice melt, thermal expansion, isostatic adjustment, and associated changes in the tidal dynamics. They use a very sophisticated tidal model with a high resolution, unstructured grid, and included wetting and drying of intertidal areas. Consequently, they produced high resolution estimates of probable future scenarios.

[5] Reconstructions of paleotidal systems have shown that the tides in the Gulf of Maine have undergone significant change over the last 7000 years [*Scott and Greenberg*, 1983; *Gehrels et al.*, 1995]. Using a paleotidal model, *Gehrels et al.* [1995] found that mean high water 7000 years ago was just over half of present-day values and 2.4–2.8 m of this increase is due to amplification of the M_2 tide caused by resonance. Tide gauge data from the last century also show significant increases in the M_2 amplitude [*Godin*, 1992; *Ray*, 2006; *Müller et al.*, 2011]. The forcing behind these changes has been somewhat elusive, although *Greenberg et al.* [2012] pointed out that SLR is likely to be a very important contributory factor.

[6] *Pelling et al.* [2013] show, using a numerical tidal model without intertidal wetting and drying, that the way SLR is implemented in a tidal model is important for how the tides responds the change in sea level. If permanent flooding of land is allowed on the European Shelf, the response of the tides to SLR is dramatically different compared to if vertical walls are introduced at the present-day coastline (referred to as "no flooding" by *Pelling et al.* [2013]). This is because the newly flooded areas will have high tidal velocities due to their shallow water depth, and consequently dissipate significant amounts of tidal energy due to bed friction. This effect shifts the amphidromic points toward the locations with enhanced dissipation [*Taylor*, 1922] and consequently alters the entire tidal regime. The introduction of high vertical walls at the present-day coastline on the other hand, which of course prevents the flooding of land, solely introduces changes in the propagation speed of the tidal wave, but may also impact on the resonant properties of the certain basins [e.g., *Arbic and Garrett*, 2010; *Green*, 2010; *Pelling et al.*, 2013].

[7] It is important to make a clear distinction here between what we call flooding/no flooding, and wetting and drying. The latter is an intertidal flooding process which consequently acts during a tidal cycle, whereas our definition of flooding/no flooding is a feature in which SLR is enough to permanently flood land cells and thus not allowing them to dry out during the tidal cycles. Flooding may of course be combined with wetting and drying: SLR is implemented (causing flooding), and during a tidal cycle, there may be a temporary wetting and drying of new and existing cells in addition to once generated due to flooding.

[8] In this paper, we will use an established tidal model, described in detail by *Egbert et al.* [2004] but using a regional setup here, to investigate the effect of free stream TPPs and SLR on the tides in the Gulf of Maine. We do not attempt to reproduce the results of [*Greenberg et al.*, 2012]—instead, we offer a study concentrating on sensitivity tests and use SLR to increase our understanding of how perturbations may affect the tidal system. We therefore look at relatively large levels of SLR and tidal power extraction to build worst-case scenarios rather than building the most realistic cases.
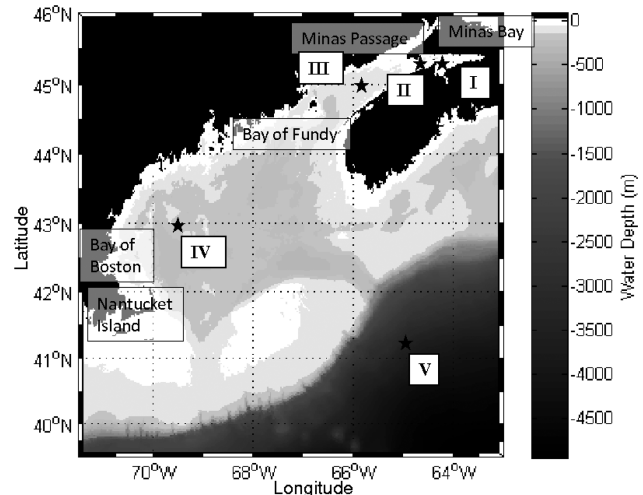
Figure 1. The bathymetry of the model domain. The black points mark the locations used to discuss results in the paper.

2. Methods

2.1. Oregon State University Tidal Inversion Software

[9] Model simulations were conducted using the Oregon State University Tidal Inversion Software (OTIS, see *Egbert et al.* [2004] for details), which was run with a horizontal resolution of 1 arc min in both latitude and longitude (see Figure 1 for the domain). The model solves the shallow water equations with rotation and bed friction:

$$\frac{\partial \mathbf{U}}{\partial t} + \mathbf{U}\dot{\nabla}\mathbf{u} + f \times \mathbf{U} = -gh\nabla(\eta - \eta_{\mathrm{SAL}}) + k\nabla^2\mathbf{U} + \mathbf{F} + \Theta \quad (1)$$

$$\frac{\partial \eta}{\partial t} = -\nabla \cdot \mathbf{U} \quad (2)$$

[10] Here, $\mathbf{U} = \mathbf{u}H$ is the depth-integrated volume transport given by the velocity $\mathbf{u}$ times the water depth H, t is time, $\mathbf{f}$ is the Coriolis vector, η and η_e are the tidal elevation and equilibrium tide, respectively, $\mathbf{F}$ is the dissipative stress from bed friction, Θ is the astronomic tide-generating force, and $k = 100\mathrm{m}^2\mathrm{s}^{-1}$ is the horizontal turbulent eddy viscosity.

[11] The bed friction is parameterized using the standard quadratic law:

$$\mathbf{F} = C_d\mathbf{U}|\mathbf{u}_t|/H \quad (3)$$

where $\mathbf{u}_t$ is the total velocity vector for all tidal constituents under consideration and $C_d = 3 \times 10^{-3}$ is a drag coefficient.

[12] Tidal elevations and phases from the TPXO7.2 database (see *Egbert and Erofeeva* [2002] and http://volkov.oce.orst.edu/tides/global.html for details) were prescribed at the open boundaries, and the astronomic tidal potential was applied over the domain. No further assimilation of data was used, thus allowing us to conduct perturbation simulations without the constraint of present-day tides. The bathymetric and topographic data was a composite data set available from http://pubs.usgs.gov/of/1998/of98–801/bathy/

index.htm. A constant self-attraction and loading correction scheme with $\beta = 0.1$ was also used [*Ray*, 1998]. The model was run using forcing for the M_2, S_2, N_2, K_1, and O_1 tidal constituents, although the results described here will mainly concentrate on the astronomic tide (defined here as the sum of the amplitudes of all five constituents and also known as mean spring high water) and the M_2 constituent. The model was run for a total of 46 days and harmonic analysis was carried out on the last 34 days to separate the M_2 and N_2 signals.

2.2. SLR and TPP

[13] After establishing a control simulation, runs were made with various levels of SLR. It was implemented in the two ways described earlier: either by increasing the water depth over the entire region and allowing low lying cells to flood (henceforth referred to as "flood run"), or by increasing the water depth but not allowing new areas to flood. The second method is analogous to building walls around the present-day coastline and is denoted the "no-flood run" in the following. Intertidal wetting and drying was not included in this investigation.

[14] Tidal-free stream tidal turbines introduce an additional drag term on the flow and it is possible to parameterize the turbines by adding an additional term (K_t) to the quadratic bottom friction formulation [e.g., *Sutherland et al.*, 2007]. From equation (3), we then get

$$\mathbf{F} = (C_d + K_t)\mathbf{U}|\mathbf{u}|/H \qquad (4)$$

[15] The power P_t associated with K_t, that is, from the turbines only, can be estimated from *Garrett and Cummins* [2005], *Sutherland et al.* [2007], *Blanchfield et al.* [2008], and *Karsten et al.* [2008]:

$$P_t = P\frac{K_t}{K_t + C_d} \qquad (5)$$

where

$$P = \rho(C_d + K_t)\overline{(u^2 + v^2)}^{3/2}A \qquad (6)$$

in which ρ is the density of sea water and A is the horizontal area covered by the tidal turbine field. As K increases so does P until, in geophysical flows, a limit is reached after which P will decrease with increasing K_t. This is because if too many turbines are placed in a channel the drag they create would slow the current and thus reduce the maximum power output of the power station. Therefore, there is a theoretical maximum to the amount of power available in a realistic application [e.g., *Garrett and Cummins*, 2005].

2.3. Control Simulation

[16] The control simulation results successfully reproduce the exceptionally high tides in the Minas Bay, dominated by the M_2 constituent (Figure 2). To evaluate the model performance, we compared the control amplitudes to those from the regional inverse tidal solutions available at http://volkov.oce.orst.edu/tides/EC.html. In the following, we refer to the regional solution as the ATLAS because it is part of the OTIS ATLAS for the North Atlantic (see http://volkov.oce.orst.edu/tides/atlas.html for details). The

root-mean-square (RMS) difference between the control run and the ATLAS is less than 7 cm for M_2. We have also calculated how well the model captures the structure of the observed field using the variance capture, $VC = 100 \times [1 - (RMS/S)^2]$, where S is the RMS of the ATLAS elevations and RMS is the RMS difference between the model and the ATLAS aforementioned. The resulting capture is $VC = 99\%$, and the accuracy of the model is thus reasonably high considering the very large range of the tides in the area. It is also similar to other simulations of the tides in the area [*Sucsy et al.*, 1993; *Dupont et al.*, 2004; *Karsten et al.*, 2008], and we argue that the model shows considerable skill in reproducing the structure of the tidal regime in the Gulf of Maine.

3. Free Stream Tidal Power Plant Results

3.1. Maximum Power Output

[17] We have incrementally increased the turbine drag term (K_t) over the Minas Passage and calculated P for each value of K_t. This way we estimate that the maximum power output for the Minas Passage is 7.1 GW and occurs when $K_t = 0.1$ and the current velocities are 1.9 ms^{-1} (Figure 3). This result is similar to other numerical and theoretical estimates for the area [e.g., *Karsten et al.*, 2008]. After this point, the maximum power output decreases exponentially, reaching zero when $K_t = 0$. This allows the maintenance of a higher power output ($P > 6$ GW) when $K_t > 0.04$, although P rapidly drops for lower levels of K_t. The current velocity decreases exponentially as P approaches its maximum, resulting in a reduction of the current velocity of some 1.3 ms^{-1} in Minas Bay.

[18] In the following, we investigate the response of the tides to two different TPP schemes. The first uses a power extraction which is slightly less than the maximum power output, or 7.1 GW. This is referred to as "large" in the following, as opposed to the "small" TPP, which operates at 75% of the maximum power output, or 5.2 GW. This corresponds to using $K_t = 0.1$ and 0.03, respectively.

3.2. Impacts of Free Stream Tidal Turbines in Minas Passage

[19] Increasing the tidal dissipation, and thus restricting the flow through Minas Passage, has large impacts on the tides in the Gulf of Maine. The impacts of both the large and small power plants are considerable and result in a decrease of the (semidiurnal) tidal amplitude within Minas Bay and an increase over the rest of the Gulf of Maine (Figure 4). The largest impacts are of course seen within the Minas Bay itself with a decrease of 2 m in M_2 amplitude for the larger power plant (extracting 7.1 GW) and 1.3 m for the smaller plant (operating at 5.2 GW). The effects extend almost out of the entrance to the bay and to the shelf edge, but do not extend to the domain boundaries. The impact for the smaller power station is, as expected, less pronounced than that of the larger TPP. In fact, the difference between the two power plants is much larger behind the turbines, with a difference of approximately 1.3 m in Minas Basin, whereas it is only some 2 cm in the Bay of Boston compared to the control.

[20] Details of the response to increased power extraction of the M_2 amplitudes at four positions in the Gulf of
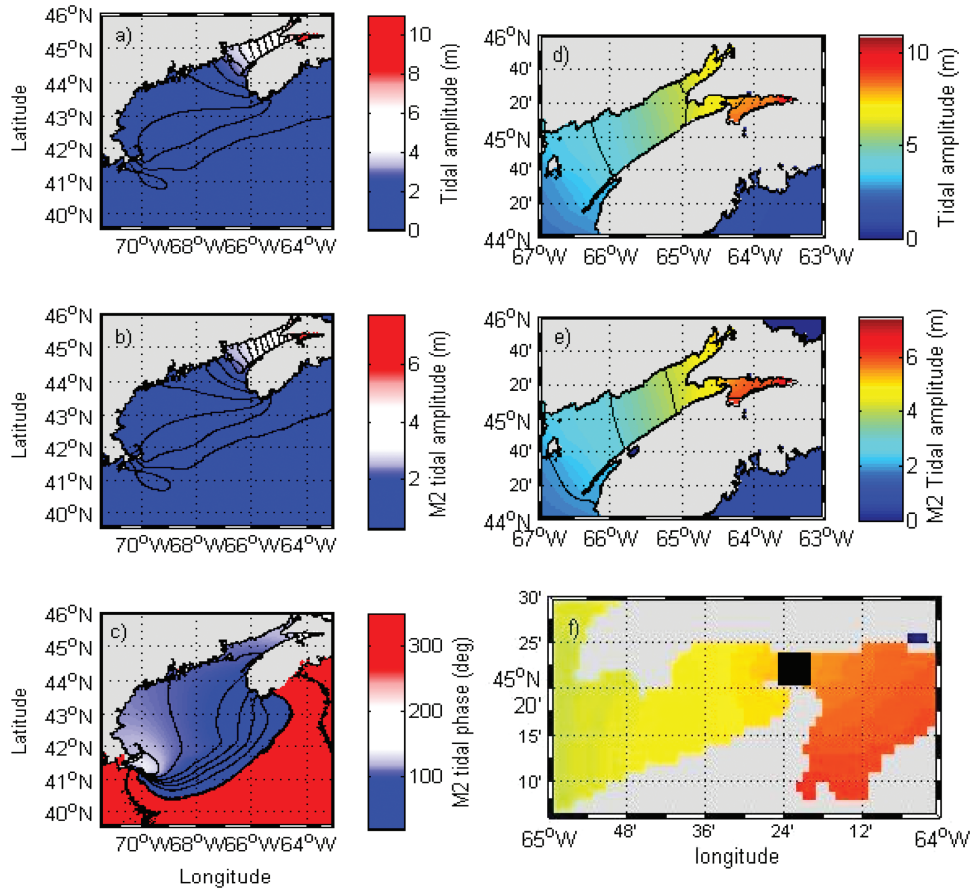
Figure 2. Simulations of present day tidal amplitude in the Gulf of Maine. (a) The astronomic tide (defined here as the sum of the M_2, S_2, N_2, K_1, and O_1 tidal amplitudes), (b) the M_2 tidal amplitude only, and (c) the phase of the M_2 tide only. (d and e) Close-up versions of Figures 2a and 2b, respectively. Please note the difference in axis limits between the plots. (f) The location of the free stream TPP is shown by a black rectangle.

Maine are shown in Figure 5 (the locations are shown in Figure 1). The response shows decreases in tidal amplitude behind the power plant and increased tides in front of it.

The exception to this is location II, which is positioned in the Bay of Fundy just in front of the power plant. The amplitude at this station decreases rapidly with increasing
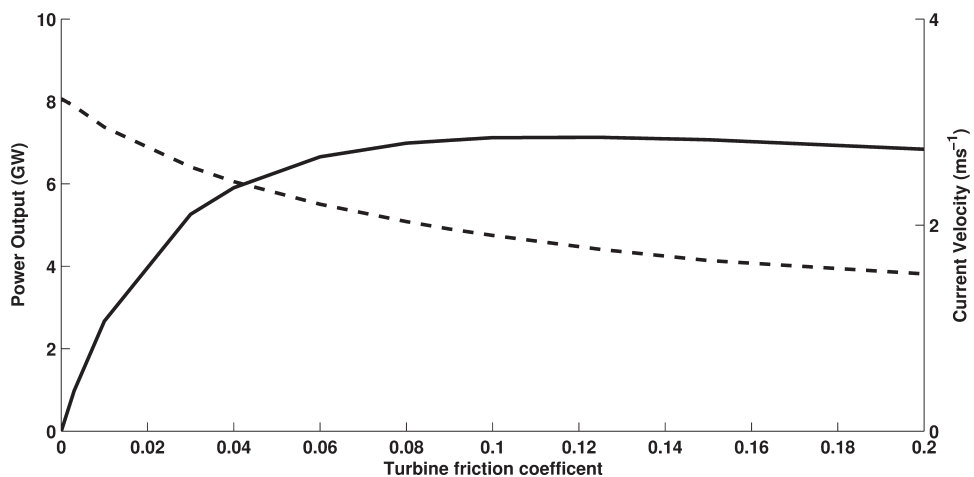
Figure 3. Power output by a TPP in Minas Passage, calculated from equation (5), shown by the solid line and left-hand axis. The associated current velocity within the TPP is shown by the dotted line and uses the right-hand axis scale.
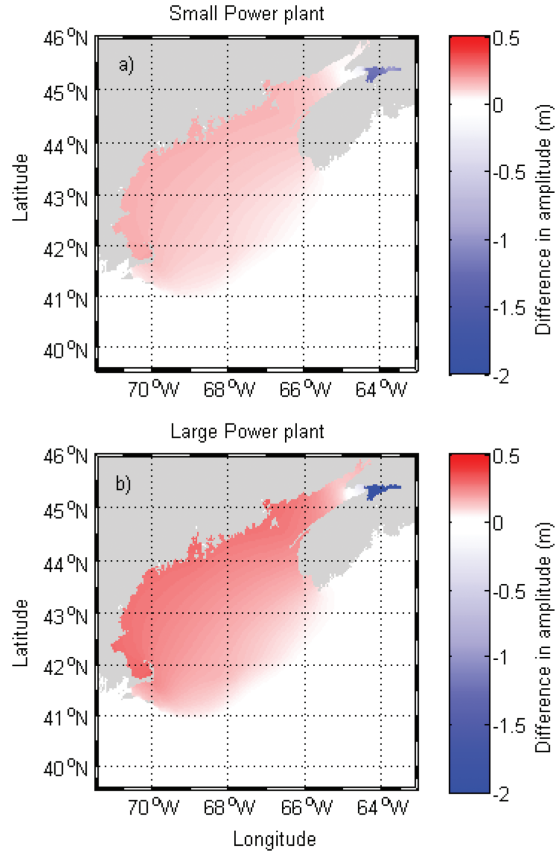
Figure 4. Impact of (a) small and (b) large TPP on the M_2 tidal amplitude in the Gulf of Maine (shown is TPP minus control amplitudes). The corresponding power output of the large and small TPP is 7.0 and 5.2 GW, respectively.

values of K_t, only to increase as K_t increases beyond $K_t = 0.075$ (Figure 5b; this is similar to the findings of *Hasegawa et al.*, 2011). We suggest that this is a result of a reflection of the tide at the TPP, when $K_t = 0.075$. Therefore, when $K_t > 0.075$, the TPP acts as a partially permeable barrier, effectively shortening the length of the basin and potentially bringing it closer to resonance [e.g., *Garrett*, 1972]. However, when $K_t < 0.075$, we suggest the reduction of amplitude is due to the removal of tidal energy after it is reflected at the head of Minas Bay.

4. SLR Results

4.1. Response to SLR

[21] The spatial response of the tides to SLR is shown in Figure 6, with the black areas in the no-flood results (Figures 6a, 6c, and 6e) showing the areas which has flooded in the flood simulations. In all simulations, the new land created by flooding is restricted to the Bay of Boston and along the coast of Halifax, in the northeast of the domain.

[22] An SLR of 1 m gives similar tidal responses for both the no-flooding and flooding scenarios (Figures 6a and 6b, respectively). Localized reductions of tidal amplitude are seen close to Nantucket, in the Southern part of the domain, in the flooding scenario but not in the no-flood run. The difference in tidal response between the two SLR

implementation methods becomes clearer with 2 and 5 m SLR (Figures 6c–6f). The extent of the changes in tidal amplitude in the flooding scenario is significantly reduced compared to the 1 m SLR case, only covering Minas Bay, whereas the no-flooding response again extends to the mouth of the Bay of Fundy. As could be expected, significantly more areas have flooded with 2 and 5 m SLR, compared to the 1 m SLR case, and this explains the difference between the responses.

[23] The response of the tides to further SLR is shown in Figure 7. The response inside Minas Bay (location I in Figure 1) clearly shows that when flooding is prohibited the bay passes through two peaks (Figure 7a). The first and smaller of the two occurs with 1 m SLR and only occurs in the astronomic tide, whereas the second maximum is more protracted and appears around the very extreme 16 m SLR. Interestingly, these two peaks do not appear in the flooding scenario, which overall has a weaker response to SLR. In these runs, there is some amplification at 16 m SLR, but this response is dampened and the amplitude reached is 2 m less than for the no-flood scenario.

[24] The tidal response to SLR in the Bay of Fundy is very similar to the response in Minas Bay (Figure 7b). The amplitude of the response of the tides to SLR decreases as we progress further outward in the basin, most likely due to the decrease of tides in that region. Again, there are two maxima in the tidal amplitudes as sea level increases in the model, but the second point is reached slightly later than in the Minas Passage, at approximately 20 m SLR. This trend in a delayed maximum is seen within the Gulf of Main Proper as well (Figure 7c). The response of the tides to SLR is structurally similar to the response in the Bay of Fundy (Figures 7b and 7a, respectively), but there is only one amplitude maximum and it appears with 25 m SLR.

[25] The present-day resonant period of the Bay of Fundy lies between 12.5 and 13.4 h depending on investigation [*Garrett*, 1972; *Greenberg*, 1979; *Godin*, 1988, 1993; *Ku et al.*, 1985], which is close to the periods of the N_2 (12.66 h) and M_2 (12.42 h) tidal constituents (shown by the shaded area in Figure 8). If we assume linear theory, resonance occurs when the basin has a length of multiples of quarter wave lengths of the tidal wave under consideration, or when $L_{basin} = 0.25\sqrt{gH}/T$ (where T is the tidal period). Using the average depth of the Bay of Fundy to be 53 m and its length to be ∼260 km (these values are based on the bathymetery data for the control simulation), we see that the basin will approach resonance as sea level increases assuming a no-flooding scenario (Figure 8).

[26] Both linear theory and our results show that we will move toward a resonant state of the Bay of Fundy with SLR, and that the bay will probably reach N_2 resonance before M_2 resonance [see also *Egbert et al.*, 2004; *Green*, 2010; *Webb*, 2012]. The tidal amplitude maxima occur for different levels of SLR in the different locations, which suggest that the resonance in the Gulf of Maine cannot be described by single-model resonance. There is also some disagreement between the model results and the tidal resonance theory shown in Figure 8, but some useful conclusions can still be drawn.

[27] The predicted SLR required to meet an N_2 resonant state from Figure 8 and the model runs compare favorably (both predict/require 1 m SLR), but the SLR required to
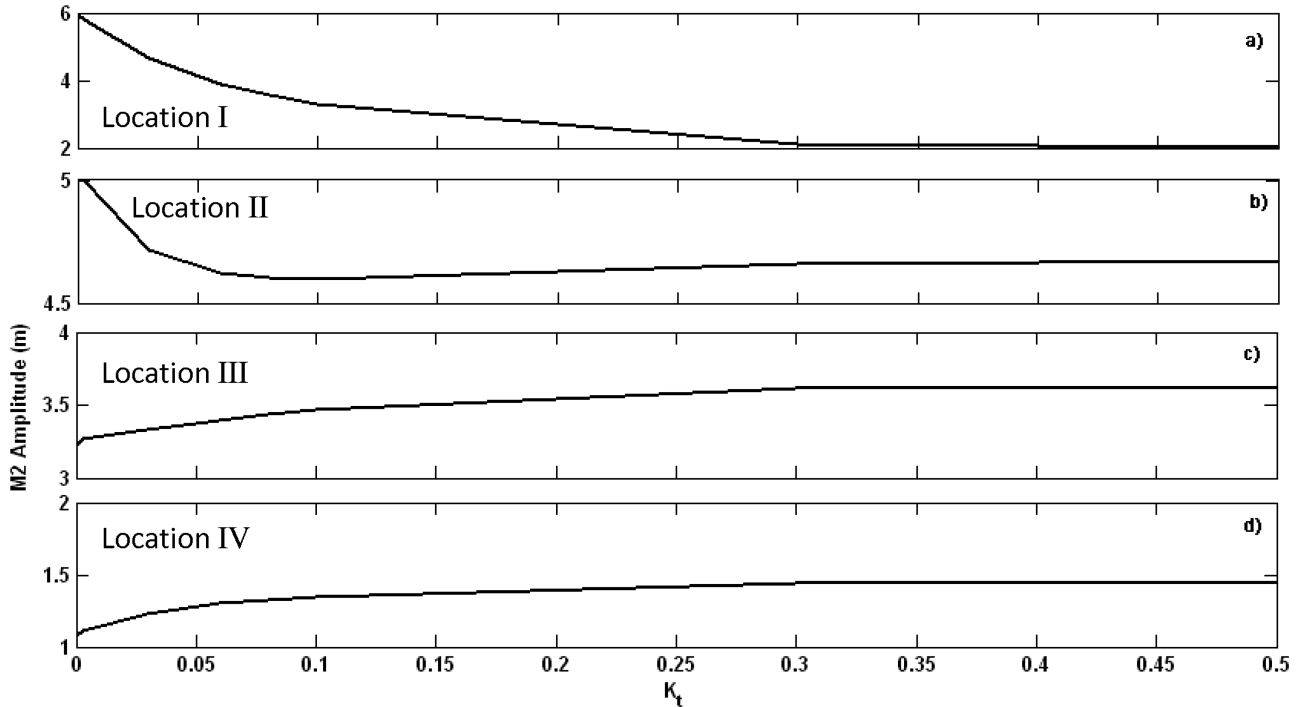
Figure 5. Response on the M_2 amplitude in the locations marked in Figure 1 of an increased turbine drag coefficient (K_t). Note the different y axis scales between panels.

reach the M_2 resonant state differs by approximately 16 m between Figure 8) and the no-flood runs. The reason for this disagreement is that as the basin approaches resonance the tidal velocities will increase, which in turn will increase the loss of tidal energy due to bed friction [see *Garrett*, 1972]. However, the velocity-dissipation relation is cubic, so a small change in velocity can lead to a very large increase in energy loss with a negative feedback on the tidal amplitudes. We can therefore expect a reduction of the M_2 tidal amplitudes, due to increased dampening, as the basin approaches resonance. This can be compared to a dampened harmonic oscillator near resonance, where the oscillation amplitude is given by

$$\partial_{tt}u + \gamma\partial_t u = \sin\,\omega t \qquad (7)$$

and the rate of energy dissipation is

$$\epsilon_H = \frac{1}{2}\Re\left[i\omega/\left(1 - i\gamma\omega - \omega^2\right)\right] \qquad (8)$$

where i and $\Re$ denote the imaginary and real parts of the equation, respectively, γ is the damping coefficient, ω is the forcing frequency, and subscript H denote the derivatives. From equations (7) and (8), we can see that as we approach resonance, increased dampening causes reduced dissipation due to reduced amplitudes (see *Egbert et al.* [2004] and *Arbic and Garrett* [2010] for a tidal analogy). However, this response is not as strong for N_2 as the N_2 tidal friction is primarily controlled by the M_2 velocity (see equation (3)) and the M_2 velocity remains dominant even when N_2 approaches resonance.

4.2. SLR and Free Stream Tidal Turbines in Minas Passage

[28] The next logical step is to combine SLR and TPP. When the power output calculations were repeated with 2 m SLR, we found that the maximum power output for the Minas Passage would increase by just over 1–8.4 GW for the flood run and increase by over 2 GW, to 9.2 GW, for the no-flood run (Figure 9). This increase is due to the increase in tidal velocities through the Minas Passage with SLR.

[29] The largest effect on the tides in the combined simulations is (not too surprisingly) seen with the large tidal power plant and 2 m no flooding implemented. The smallest impact on the tides is consequently found with the small power plant and a 2 m flood implementation (Figure 10), but in both cases the effect of SLR is actually surpassed by the impact of the turbines, and there does not appear to be any nonlinear effect of adding the two processes. The difference of the impacts between the three scenarios (TPP only, and TPP and 2 m SLR with flooding and without flooding) are largest in the stations closest to the power plant (stations I and II in Figure 1; Figures 11a and 11b).

5. Discussion

[30] We have used a suite of simulations to calculate the maximum power output of the Minas Passage, impact of a free stream tidal power plant in Minas Passage, and evaluate how this changes with SLR. We have also simulated the tides of the Gulf of Maine with extreme levels of SLR to investigate the resonance properties of the basin.
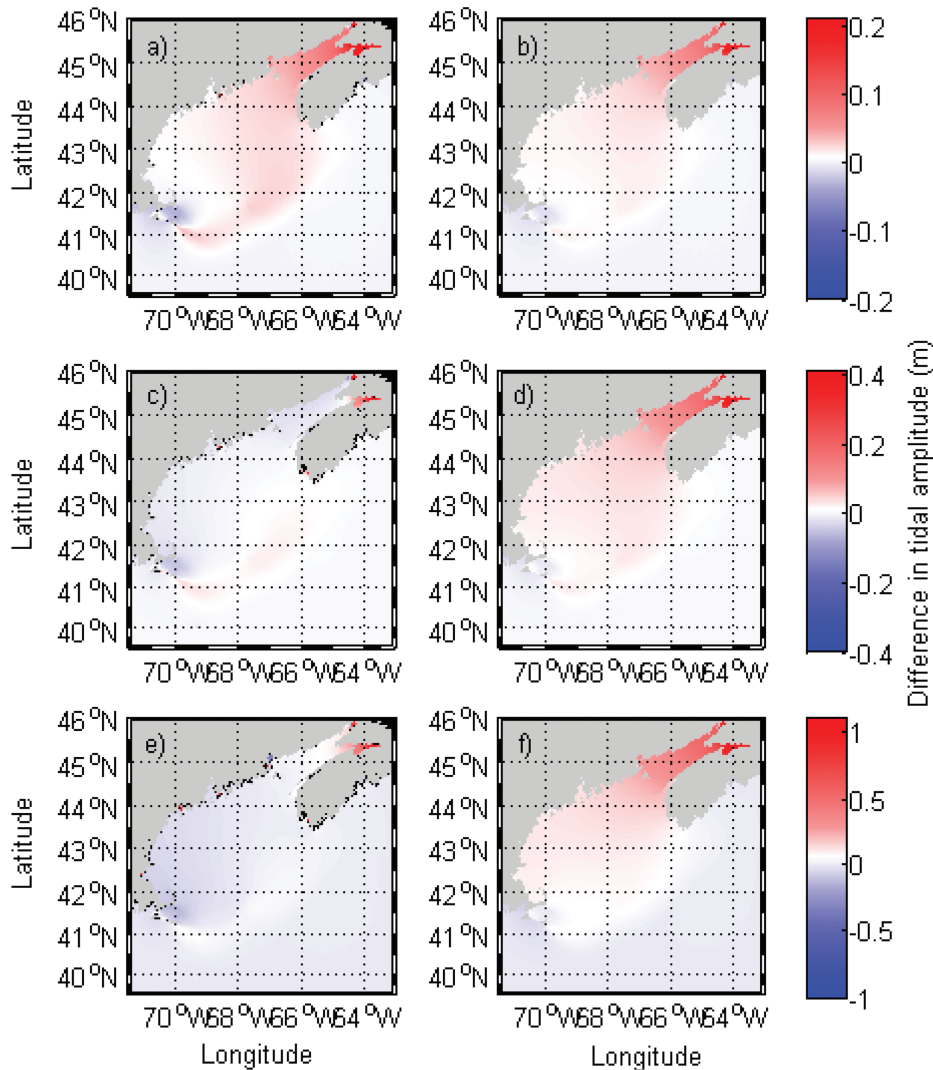
Figure 6. Spatial response (in meters) of the astronomic tidal range to SLR in the Gulf of Maine. SLR values (a and b) 1, (c and d) 2, and (e and f) 5 m, with panels on the left showing results from the flood runs and panels on the right showing the no-flood simulations. Black areas in Figures 6a, 6c, and 6e depict areas that have flooded in Figures 6b, 6d, and 6f. Note that the limits of the color scale are proportional to the level of SLR in each panel.

[31] The maximum power available for extraction from a free stream tidal power plant in Minas Passage is estimated to be 7.1 GW. Our results also show significant impacts of free stream tidal power plants in the Minas Passage that extend throughout the Gulf of Maine. There have been a number of studies which calculate the present-day maximum power output of the Minas Passage along with the impact on the regional tides, and our results fall within these estimates. For technical reasons, we show the impact of removing energy from the whole of the water column. However, studies have shown that removing energy from only the bottom half of the water column may reduce the feedback effects on the tides [*Hasegawa et al.*, 2011].

[32] The permanent flooding of new land significantly alters the response of the tides to SLR in the Gulf of Maine. Due to their shallow water depth, newly flooded areas will have high tidal velocities and consequently dissipate significant amounts of tidal energy due to friction. This increase

in dissipation appears to make the system less sensitive to resonant effects, as the flooding increases the dampening, which moves the system away from resonance (Figure 8). In the no-flood runs, no new shallow areas are produced and the increase in water depth significantly alters the resonant state of the basin. Thus, the tidal response to SLR in the Gulf of Maine is significantly stronger when flooding is restricted. Furthermore, there are back effects which reach the Bay of Boston, but no effects of SLR reach off-shelf and thus the boundary forcing remained the same in each of the SLR runs. This is supported by the global simulations presented by *Green* [2010], who show that a 5 m SLR would result in an average increase of the tidal amplitudes at the boundary of 3.6 cm. When looking at moderate and realistic levels of SLR, that is, less than $\approx$ 2m, the use of present-day boundary conditions is thus valid.

[33] The results presented here fall in line with the many studies that demonstrate the sensitivity of the Gulf of
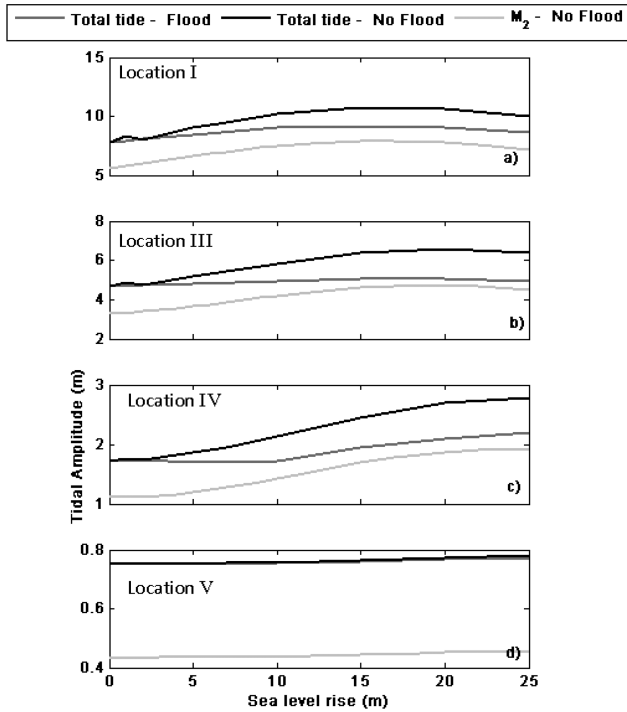
Figure 7. The change in tidal amplitude as a function of SLR at the four stations shown in Figure 1. The black (dark gray) line shows the astronomic tide without (with) flooding, whereas the light gray line shows the response of the M_2 constituent without flooding. Note the different amplitude scales between panels.

Maine system to perturbation due to the close proximity of the basin to resonance [*Garrett*, 1972; *Ku et al.*, 1985; *Godin*, 1993; *Gehrels et al.*, 1995; *Karsten et al.*, 2008].
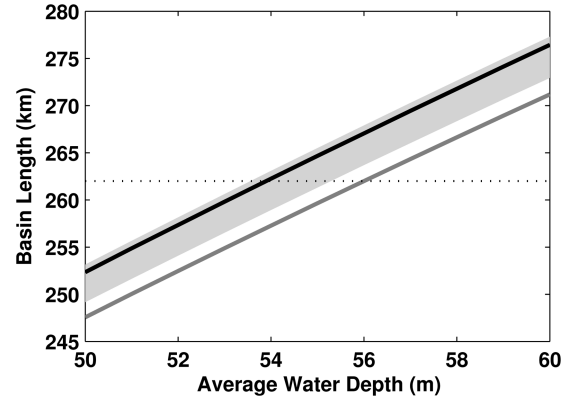

Figure 8. The necessary basin length (L_{basin}) as a function of average water depth for tidal resonance to occur within the Bay of Fundy. The gray and black lines show the basin length and average water depth combination which gives resonance for N_2 (black line) and M_2 (gray line). The estimated natural frequencies as estimated by *Godin* [1988] are shown as the gray patch. Horizontal dotted line shows the length of the basin in the present day bathymeteric database used for the numerical simulation.

Although previous investigations have suggested that SLR will bring the Bay of Fundy closer to resonance—and hence increase the tidal amplitudes there [e.g., *Garrett*, 1972]—few dynamic studies of the region's response to SLR have taken place. However, our results do agree with suggested implications in *Gehrels et al.* [1995], who show that although mean high water increased by 33.6 m over the last 7000 years, only some 8% of this was due to an amplification of the M_2 tide, suggesting that the resonance
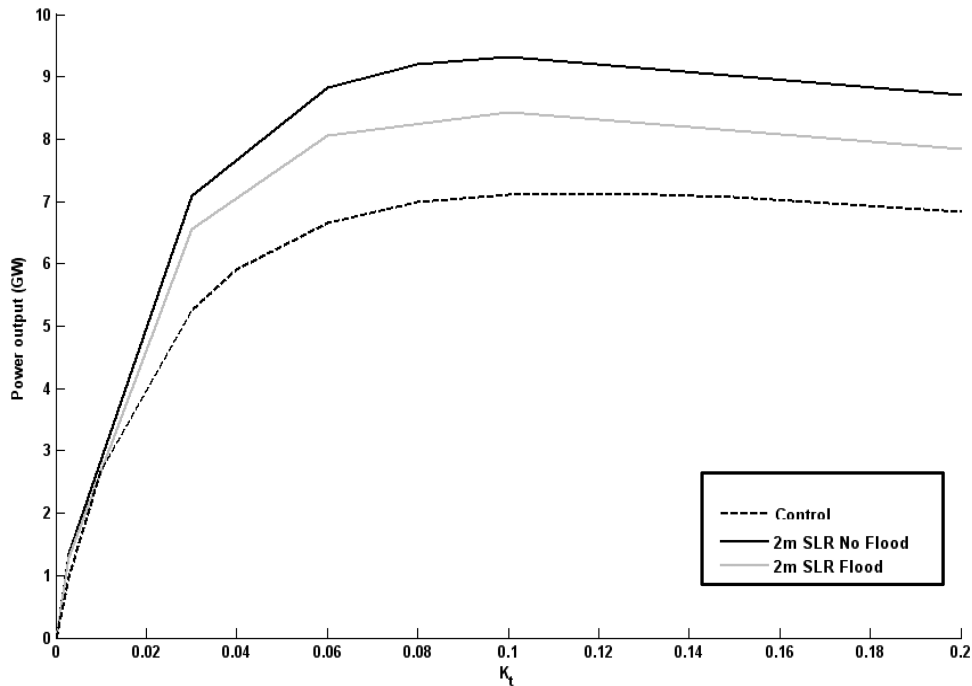
Figure 9. Maximum power output (in GW) for a free stream TPP in Minas Passage as a function of turbine friction, K_t. The control results are shown in solid black, whereas gray and dashed lines show the response with 2 m SLR for the flooding and no-flooding cases, respectively.
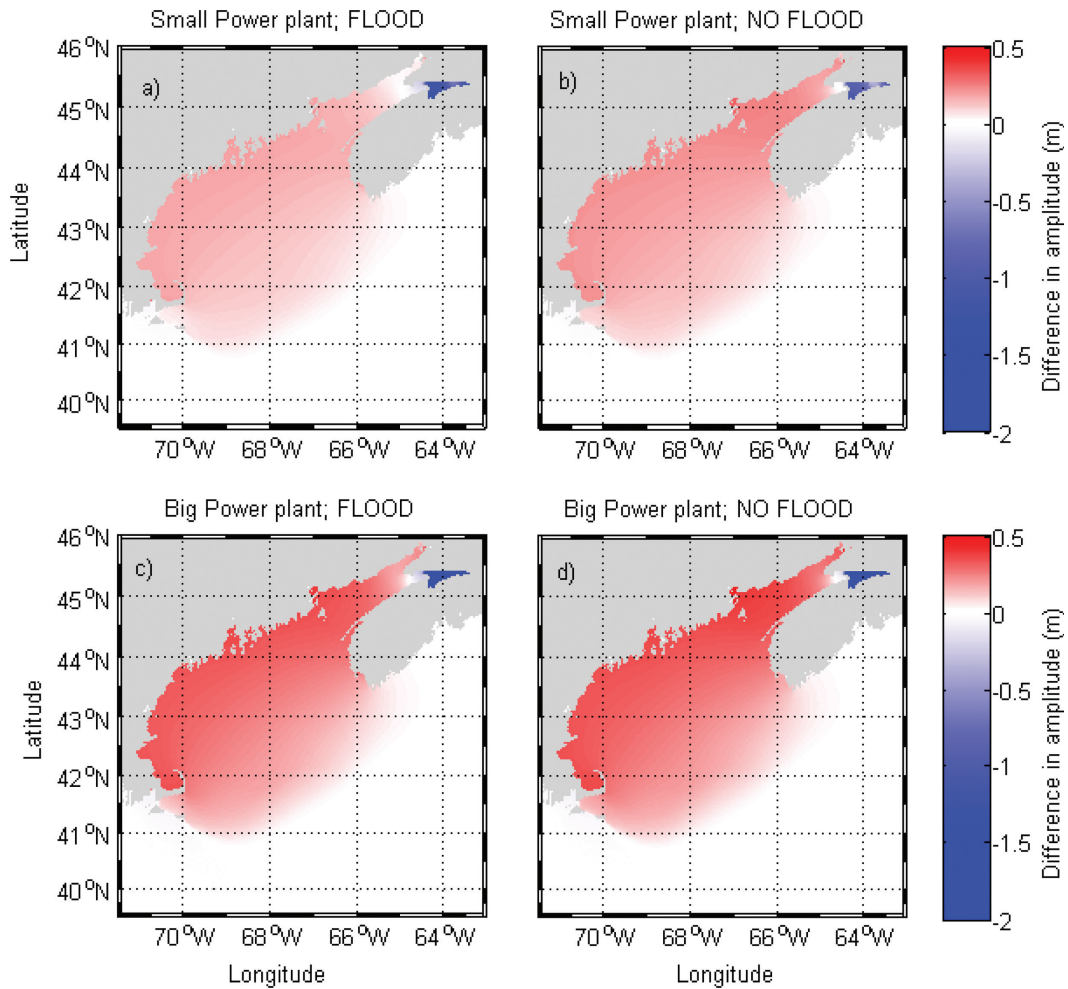
Figure 10. Impact of a combination of large and small TPP and 2 m SLR (a and c) with flooding and (b and d) without flooding. Note the skewed color bar range (white is 0 difference) and that we again show results from perturbation runs minus the control.
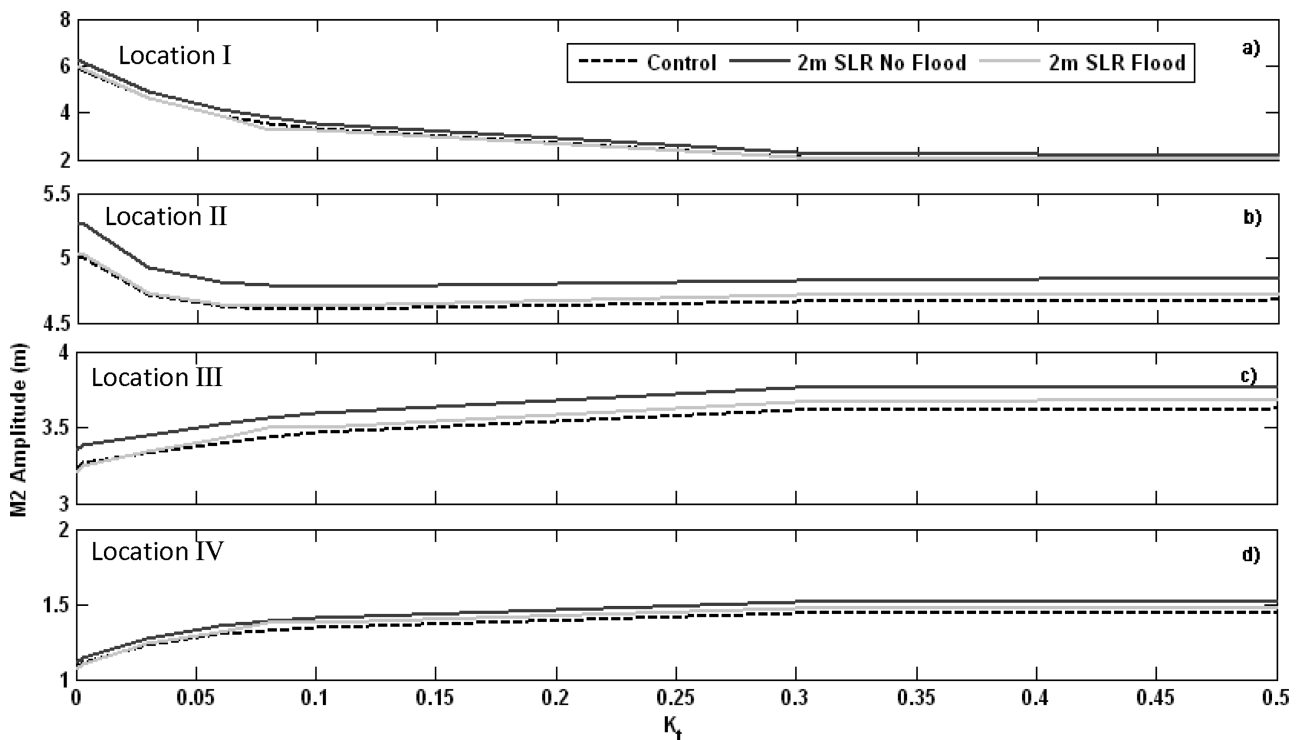
Figure 11. Response of the M$_2$ amplitude to an increased turbine drag coefficient, K_t, in combination with 2 m SLR at the location shown in Figure 1.

was dampened by flooding. The results in *Greenberg et al.* [2012] also suggest that high water is expected to increase in the Bay of Fundy over the next century due to SLR and associated increases in tidal amplitudes. Our results also compare qualitatively well to tide gauge observations, which show that the M_2 amplitude has increased over the past century (during which the area has experienced SLR *Greenberg et al.* [2012]). However, if (as our results suggest) flooding is important to the response of the tides to SLR, investigating the past rate of change of the tides may not be all that useful, as it becomes crucial to analyze the changes in flooding areas and thus bathymetery/topography.

[34] We have used a relatively simplistic tidal model which is computationally cheap. However, an RMS difference of 7 cm was still achieved when comparing the control M_2 amplitudes to those from the ATLAS. It was also found that including wetting and drying actually increased the model error, most likely due to the coarse resolution of the intertidal area when compared to an unstructured grid [e.g., *Greenberg et al.*, 2012]. Although it is arguable that a more sophisticated model may increase the model accuracy, we would suggest that the model setup we have used is more than capable for the identification of dynamic processes and sensitivities, but we do concede that for realistic predictions a higher resolution model should be used. Also, only mean SLR has been implemented here, which means we have ignored any isostatic impact. Isostatic (or relative) sea level change will, no doubt, have additional effects on the tidal system of the Gulf of Maine [see *Greenberg et al.*, 2012].

[35] The Minas Passage is a highly attractive area for the extraction of free stream tidal energy, and with growing interest in renewable energy methods this interest is likely to increase. However, the impacts on the tidal regime by large-scale TPP are significant and far reaching. There are also additional impacts resulting from changes to the tidal system, for example, increased flooding, changes to sediment transport pathways, and changes to the ecological system. It also follows that if future SLR brings the basin closer to resonance, the maximum tidal power output will increase and the present investigation is the first study to model this directly. Because TPPs are designed to have a long-working life ($+100$ years), it is likely that they will operate under conditions with changed sea level, and it is shown here that there is an important combined impact of TPPs and SLR on the Bay of Fundy.

[36] Many developed countries have flood defense plans in place to try and protect large cities and towns from rising sea level. However, little is known about how these flood defenses will affect the oceanic response to SLR at a basin scale. The present paper highlights how the addition of basin scale flood defense systems, that is, the equivalent of a no-flood run, can introduce significant effects on regional tidal dynamics in some regions, but that the response varies significantly between basins. In fact, to a large extent the Gulf of Maine, and especially the Bay of Fundy itself, responds in the opposite way to the European Shelf where the largest changes in tidal amplitudes with SLR is found for flood scenarios [*Ward et al.*, 2012; *Pelling et al.*, 2013]. The combined impact of SLR and tidal power plants highlight the need to investigate at not just how TPP impacts the tidal system at the present day, but also how the tidal system might change in the future.

References

Arbic, B., and C. Garrett (2010), A coupled oscillator model of shelf and ocean tides, *Cont. Shelf Res.*, *30*, 564–574.

Blanchfield, J., C. Garrett, P. Wild, and A. Rowe (2008), The extractable power from a channel linking a bay to the open ocean, *Proc. Inst. Mech. Eng., A J. Power. Energy*, *222*, 289–297.

Church, J., and N. White (2006), A 20th century acceleration in global sea-level rise, *Geophys. Res. Lett.*, *33*, L01602, doi:10.1029/2005GL024826.

Church, J., and N. White (2011), *Sea-level rise from the late 19th to the early 21st century*, Surv. Geophys., *32*, 585–602, doi:10.1007/s10712-011-9119-1.

Denman, K., et al. (2007), Couplings between changes in the climate system and biogeochemistry, in *Climate Change 2007: The Physical Science Basis. Contribution of Working Group I to the Fourth Assessment Report of the Intergovernmental Panel on Climate Change*, edited by S. Solomon et al., Cambridge Univ. Press, Cambridge, U. K.

Dupont, F., C. Hannah, and D. Greenberg (2004), Modelling the sea level of the upper Bay of Fundy, *Atmosph.- Ocean*, *43*, 33–47.

Egbert, G., and S. Erofeeva (2002), Efficient inverse modeling of barotropic ocean tides, *J. Atmos. Ocean. Technol.*, *19*, 183–204.

Egbert, G. D., B. G. Bills, and R. D. Ray (2004), Numerical modeling of the global semidiurnal tide in the present day and in the last glacial maximum, *J. Geophys. Res.*, *109*, C03003, doi:10.1029/2003JC001,973.

Garrett, C. (1972), Tidal resonance in the Bay of Fundy and Gulf of Maine, *Nature*, *238*, 441–443.

Garrett, C., and P. Cummins (2005), The power potential of tidal currents in channels, *Proc. R.. Soc.*, *461*, 2563–2572.

Gehrels, W., D. Belknap, B. Pearce, and B. Gong (1995), Modeling the contribution of M_2 tidal amplification to the Holocene rise of mean high water in the Gulf of Maine and the Bay of Fundy, *Maine Geol.*, *124*, 71–85.

Godin, G. (1988), The resonance period of the Bay of Fundy, *Cont. Shelf Res.*, *8*, 1005–1010.

Godin, G. (1992), Possibility of rapid changes in the tide of the Bay of Fundy, based on a scrutiny of the records from Saint John, *Cont. Shelf Res.*, *12*, 327–338.

Godin, G. (1993), On tidal resonance, *Cont. Shelf Res.*, *13*, 89–107.

Green, J. (2010), Ocean tides and resonance, *Ocean Dyn.*, *60*, 1243–1253.

Greenberg, D. (1979), A numerical model investigation of tidal phenomena in the Bay of Fundy and Gulf of Maine, *Mar. Geod.*, *2*, 161–187.

Greenberg, D., W. Blanchard, B. Smith and E. Barrow (2012), Climate change, mean sea level and high tides in the Bay of Fundy, *Atmos. Ocean*, *50*, 261–276.

Hasegawa, D., J. Sheng, D. Greenberg, and K. Thompson (2011), Far-field effects of tidal energy extraction in the Minas Passage on tidal circulation in the Bay of Fundy and Gulf of Maine using a nested-grid costal circulation model, *Ocean Dyn.*, *61*, 1845–1868.

Karsten, R., J. McMillan, M. Lickley, and R. Haynes (2008), Assessment of tidal current energy in the Minas Passage, Bay of Fundy, *Proc. IMechE, Part A: J. Power Energy*, *222*, 493–507, doi:10.1243/09576509JPE555.

Ku, L., D. Greenberg, C. Garrett, and F. Dobson (1985), Nodal modulation of the lunar semidiurnal tide in the Bay of Fundy and Gulf of Maine, *Science*, *230*, 69–71.

Müller, M. (2011), Rapid changes in semi-diurnal tides in the North Atlantic since 1980, *Geophys. Res. Lett.*, *38*, L11602, doi:10.1029/2011GL047312.

Müller, M., B. Arbic, and J. Mitrovica (2011), Secular trends in ocean tides: observations and model results, *J. Geophys. Res.*, *116*, C05013, doi:10.1029/2010JC006387.

Pelling, H., J. Green, and S. Ward (2013), Tides and sea level rise: to flood or not to flood, *Ocean Modell.*, *63*, 21–29.

Pickering, M., N. Wells, and K. Horsburgh (2012), The impact of future sea-level rise on the European Shelf tides, *Cont. Shelf Res.*, *35*, 1–15, doi:10.1016/j.csr.2001.11.011.

Rahmstorf, S. (2007), A semi-empirical approach to projecting future sea-level rise, *Science*, *315*, 368–370, 10.1126/science.1135,456.

Ray, R. (1998), Ocean self-attraction and loading in numerical tidal models, *Mar. Geod.*, *21*, 181–192.

Ray, R. (2006), Secular changes of the M_2 tide in the Gulf of Maine, *Cont. Shelf Res.*, *26*, 422–427.

Scott, D., and D. Greenberg (1983), Relative sea-level rise and tidal development in the Fundy tidal system, *Can. J. Earth Sci.*, *20*, 1554–1564.

Sucsy, P., B. Pearce, and V. Panchang (1993), Comparison if two- and three-dimensional model simulation of the effect of a tidal barrier on the Gulf of Maine tides, *J. Phys. Oceanogr.*, *23*, 1231–1248.

Sutherland, G., M. Foreman, and C. Garrett (2007), Tidal current energy assessment for Johnstone Strait, Vancouver Island, *Proc. IMechE, Part A: J. Power Energy*, *221*, 147–157.

Taylor, G. (1922), Tidal oscillations in gulfs and rectangular basins, *Proc. London Math. Soc.*, *20*, 148–181.

Ward, S., J. Green, and H. Pelling (2012), Tides, sea-level rise and tidal power extraction on the European shelf, *Ocean Dyn.*, *62*, 1153–1167.

Webb, D. (2012), On the shelf resonances of the Gulf of Carpentaria and the Arafura Sea, *Ocean Sci.*, *8*, 733–750.

Woodworth, P., N. Teferle, N. Bingley, R. Sherman, and S. Williams (2009), Trends in UK tidal guages revisited, *Geophys. J. Int.*, *179*, 19–30.

Woodworth, P., M. Menendez, and W. Gehrels (2011), Evidence for century-timescale acceleration in mean sea levels and for recent changes in extreme sea levels, *Surv Geophys.*, *32*, 603–618, doi: 10.1007/s10712-011-9112-8.

Woollcombe-Adams, C., M. Watson, and T. Shaw (2009), Severn barrage tidal power project: implications for carbon emissions, *Water Environ. J.*, *23*, 63–68.